ACS APPLIED MATERIALS & INTERFACES

Research Article

www.acsami.org

CdS-Decorated ZnO Nanorod Heterostructures for Improved Hybrid Photovoltaic Devices

Tamita Rakshit,[†] Suvra P. Mondal,[‡] Indranil Manna,[§,∥] and Samit K. Ray*[,‡]

[†]Advanced Technology Development Centre, [‡]Department of Physics & Meteorology, and [§]Department of Metallurgical and Materials Engineering, IIT Kharagpur, 721 302, India

[∥]CSIR-Central Glass and Ceramic Research Institute, Kolkata 700 032, India

ABSTRACT: Cadmium sulfide (CdS)-decorated zinc oxide (ZnO) nanorod heterostructures have been grown by a combination of hydrothermal and pulsed laser deposition techniques. Hybrid photovoltaic devices have been fabricated with CdS modified and unmodified ZnO nanorods blended separately with regioregular poly(3-hexylthiophene) (P3HT) polymer as the active layer. The solar cell performance has been studied as a function of ZnO concentration and the casting solvent (chlorobenzene, chloroform, and toluene) in the unmodified ZnO:P3HT devices. The power conversion efficiency is found to be enhanced with the increase of ZnO concentration up to a certain limit, and decreases at a very high concentration. The surface modification of ZnO nanorods with CdS leads to an increase in the open circuit voltage and short-circuit current, with enhanced efficiency by 300% over the unmodified ZnO:P3HT device, because of the cascaded band structure favoring charge transfer to the external circuit.

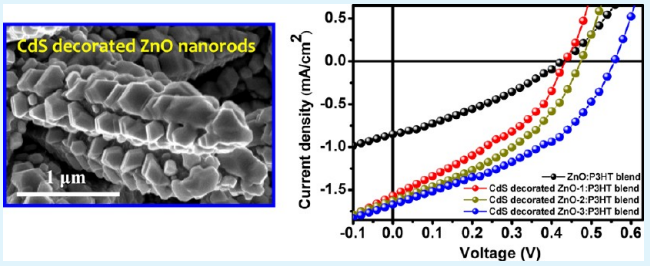

KEYWORDS: *solar cells, organic-inorganic heterojunctions, ZnO nanorods, CdS-ZnO heterostructure, photoluminescence quenching*

INTRODUCTION

Solar cells based on organic materials have drawn much attention because of their cost effectiveness. But low carrier mobility and small exciton diffusion length of organic materials reduce the efficiency for charge collection and thus limit the performance of the above solar cells.[1,2] This problem can be overcome by fabricating hybrid polymer/inorganic solar cells, because the charge transfer favorably occurs between high electron affinity inorganic semiconductors and the relatively low ionization potential polymers.[3,4] Such solar cells have the combined merits of both the materials, e.g., the low-cost solution processing capability of the organic semiconductors together with the high carrier mobility, thermal and ambient stability, and high electron affinity of the inorganic semiconductors. Different inorganic nanostructures of ZnO,[5,6] TiO_2,[7,8] CdSe,[9,10] PbS,[11] Si,[12] etc., have been successfully employed for the fabrication of hybrid solar cells. Among these, ZnO nanostructures, attractive for their different morphologies, have been widely used for fabricating solar cell devices because of their high band gap, high electron mobility, nontoxicity, and environment friendly properties. Briseno et al.[13] studied the photovoltaic properties of organic/ZnO core-shell nanowire devices and obtained a maximum efficiency of 0.036%. Bhat et al.[14] fabricated air stable hybrid solar cell with efficiency of 1.02%, using ZnO nanoparticle film as an electron selective layer and P3HT-ZnO nanoparticle blend as the active layer in an inverted device configuration. ZnO nanostructures are also useful for dye-sensitized solar cell (DSSC) applications.[15] When the surface of ZnO nanorods was modified with a dye, tetra(4-carboxyphenyl)porphyrin (TCPP), it was found that the low concentration of the dye enhanced the open circuit voltage and fill factor, but a further increase in concentration reduced the solar cell performance.[16] Erten-Ela et al.[17] fabricated hybrid solar cells consisting of perylene monoimide-monoanhydride (PMIMA) dyes with ZnO nanorod electrodes and studied the spacer properties of side chain of PMIMA derivatives. Lee et al.[18] fabricated and analyzed hybrid solar cells based on P3HT and ZnO nanoparticle bulk heterojunctions combined with ZnO nanorod arrays, in which dye molecules assisted the dispersion of ZnO nanoparticles in P3HT. However, in spite of the success of dye-sensitized solar cells, there is a need of finding some alternative cheap and stable photosensitizers for the further improvement of the performance, device stability, and reducing the cost of the solar cells.

Inorganic semiconductors for example PbS,[19,20] CdSe,[21,22] Bi_2S_3,[23] InP,[24] CdS,[25,26] etc., are attractive for the above purpose. They have several advantages over the dyes in terms of better stability; particle size tunable absorption edge to match the solar spectrum better; and can also generate multiple electron-hole pairs per photon.[22,27] Among these, CdS has been found to be attractive due to its potential applications in optoelectronic devices such as light emitting diodes, lasers, transistors, etc.,[28,29] and has been studied for photovoltaic and

Received: August 20, 2012
Accepted: October 19, 2012
Published: October 19, 2012

photosensitive devices.[30,31] Modification of the surface of ZnO nanostructures with CdS led to an enhancement in ultraviolet photoconductivity,[32] and also exhibited stable and high photocatalytic activity for water splitting into hydrogen.[33] The introduction of CdS nanostructures on ZnO surface in P3HT polymer based hybrid solar cell forms a cascaded band structure.[34] This would reduce the charge recombination at the donor−acceptor heterojunction and also increase the solar absorption, because CdS has band gap in the visible range (~2.4 eV). Moreover, the photogenerated excitons produced in CdS will generate more carriers which should also contribute to the photocurrent. Luan et al.[35] showed that a higher efficiency has been obtained with ZnO nanorods co-sensitized with both CdS and CdSe quantum dots, which further improved by introducing a layer of Al_2O_3 prior to the anchoring of the quantum dots. ZnO/CdS core−shell nanostructures has also been used as a photoanode[36−38] in a photoelectrochemical cell. But the photovoltaic measurements, which need to be carried out in an electrolyte solution[36,37] (or the electrolyte injected into the solar cells[38]), is a concern for practical applications.

In this paper, we report on the fabrication of hybrid solar cell consisting of CdS decorated ZnO nanorods:P3HT as the active layer. The optical and photovoltaic properties of the above structure have been studied in comparison to the unmodified ZnO:P3HT devices. We also report a systematic study on the solar cell performance of the unmodified device as a function of ZnO concentration and the casting solvent (chlorobenzene, chloroform, and toluene).

EXPERIMENTAL DETAILS

ZnO nanostructures were grown on copper substrates by hydrothermal method following experimental procedure reported elsewhere.[39] In brief, a reaction solution, prepared by taking 6 mL of ammonia (25%) and 120 mL of zinc chloride solution ($ZnCl_2$, 0.1M) with pH value maintained to 10.0, was poured into bottles with autoclavable screw caps. The substrates were then placed vertically dipped into the solution. These closed bottles were heated at 95 °C for duration of 90 min, and then allowed to cool to room temperature thereafter. The samples were taken out of the solution as soon as they reached room temperature, and washed thoroughly with de-ionized (DI) water. On drying in air, the substrates were found to be covered with a white layer of ZnO. CdS nanoparticles were deposited on ZnO nanostructures by pulsed laser deposition (PLD) technique. For this purpose, a target of CdS of high purity (99.999%) was used. The ZnO-coated copper substrate was placed at a distance of 4 cm from the CdS target. The target was ablated using a KrF excimer laser (λ = 248 nm, τ = 25 ns) at an energy density of ~2 J/cm^2. The deposition was carried out at 500 °C in vacuum for three different time periods of 10, 20, and 30 min, with the repetition rate of 5 Hz.

For fabricating solar cells, cleaned ITO coated glass substrates with sheet resistance of 10.0 Ω/□ were used. A thin layer of poly(3,4-ethylene dioxythiophene):poly(styrene sulfonate) (PEDOT:PSS) (Aldrich) conductive polymer for hole collection was spin coated on the ITO/glass substrates, followed by annealing at 120 °C for 10 min in air. For the preparation of the active layer, first a solution was prepared by dissolving regioregular poly(3-hexylthiophene) (P3HT) (Aldrich) at a concentration of 10 mg/mL separately in three different types of solvents, e.g., chlorobenzene, chloroform, and toluene. Then the ZnO nanostructures were lifted off from the copper substrates and dissolved separately in the above three solvents containing P3HT. In each solvent, five different concentrations of ZnO were used resulting in ZnO:P3HT composite with weight ratio of 0.5:1, 1:1, 2.5:1, 5:1, and 12:1. For the fabrication of CdS decorated ZnO:P3HT hybrid device, three CdS decorated ZnO nanostructured samples of varying deposition time of CdS were dissolved separately in chloroform solvent containing P3HT, resulting in CdS decorated ZnO:P3HT composite with a weight ratio of 5:1 in each case. This mixture of P3HT and CdS decorated ZnO nanostructures (only ZnO for control devices) were spin-coated on the PEDOT:PSS layer, and then baked at 160 °C for 10 min in air to remove the solvent. Al was deposited as the top electrode by thermal evaporation using a shadow mask of area 0.2 × 0.2 cm^2. The schematic diagram of the fabricated hybrid device is shown in Figure 1.

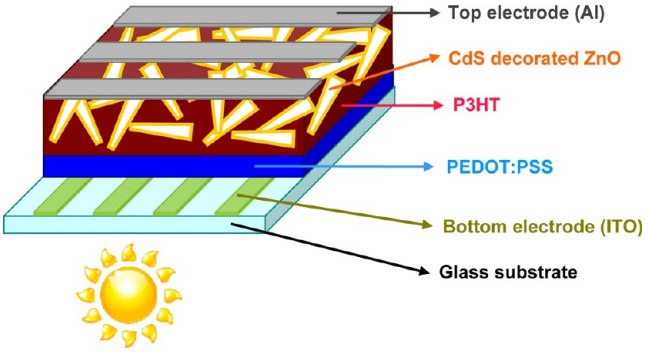

Figure 1. Schematic device structure of hybrid polymer CdS modified ZnO:P3HT blend, sandwiched between bottom contact ITO and top contact Al.

The morphology of the grown nanostructures was analyzed using a field-emission scanning electron microscope (ZEISS SUPRA 40) equipped with energy-dispersive X-ray analyzer, and a transmission electron microscope (JEOL JEM - 2100) operated at 200 kV. The phase of the grown nanostructures was studied by X-ray diffraction (XRD) (Philips X-Pert MRD) at a grazing incidence mode using Cu Kα radiation (45 kV, 40 mA). The chemical bonding of CdS decorated ZnO nanostructures was studied using X-ray photoelectron spectroscopy (XPS). XPS spectra were recorded on a PHI 5000 Versa Probe II (ULVAC − PHI, INC, Japan) system using a microfocused (100 μm, 25 W, 15 KV) monochromatic Al−Kα source ($h\nu$ = 1486.6 eV), a hemispherical analyzer, and a multichannel detector. The typical vacuum in the analysis chamber during the measurements was in the range of 1 × 10^{-10} Torr. Charge neutralization was used for all measurements using a combination of low energy Ar^+ ions and electrons. The binding energy scale was charge referenced to the C 1s at 284.6 eV. Elemental compositions were determined from the spectra acquired at pass energy of 117.4 eV. High-resolution spectra were obtained with analyzer pass energy of 29.35 eV at the step of 0.2 eV and 50 ms time per step. Ar^+ ion gun has been used. Optical absorption spectra were recorded by Perkin-Elmer Lamda 45 spectrophotometer. Photoluminescence (PL) measurements at room temperature were carried out with a He−Cd laser as an excitation source of wavelength 325 nm with an output power of 45 mW and a TRIAX 320 monochromator fitted with a cooled Hamamatsu R928 photomultiplier detector. Current−voltage (I−V) characteristics of the fabricated devices were measured using a Keithley 4200-SCS measurement unit along with a Newport 67005 solar simulator under AM 1.5 (100 mW/cm^2) solar irradiation conditions. For the photocurrent measurements at short-circuit condition, a lock-in amplifier (Standford research system-SR830 DSP) was used with a chopping frequency of 110 Hz during illumination of the samples with monochromatic light from a broad band source.

RESULTS AND DISCUSSION

Images a and b in Figure 2 show the FESEM images of the grown ZnO nanostructures on the copper substrate at different magnifications. A high density of randomly oriented nanorods, having hexagonal rod base with a gradually diminishing tip diameter, is found to be formed all over the substrate. The length of these nanorods is 1−2 μm with tip diameter of about 100−170 nm. HRTEM was carried out to further study the

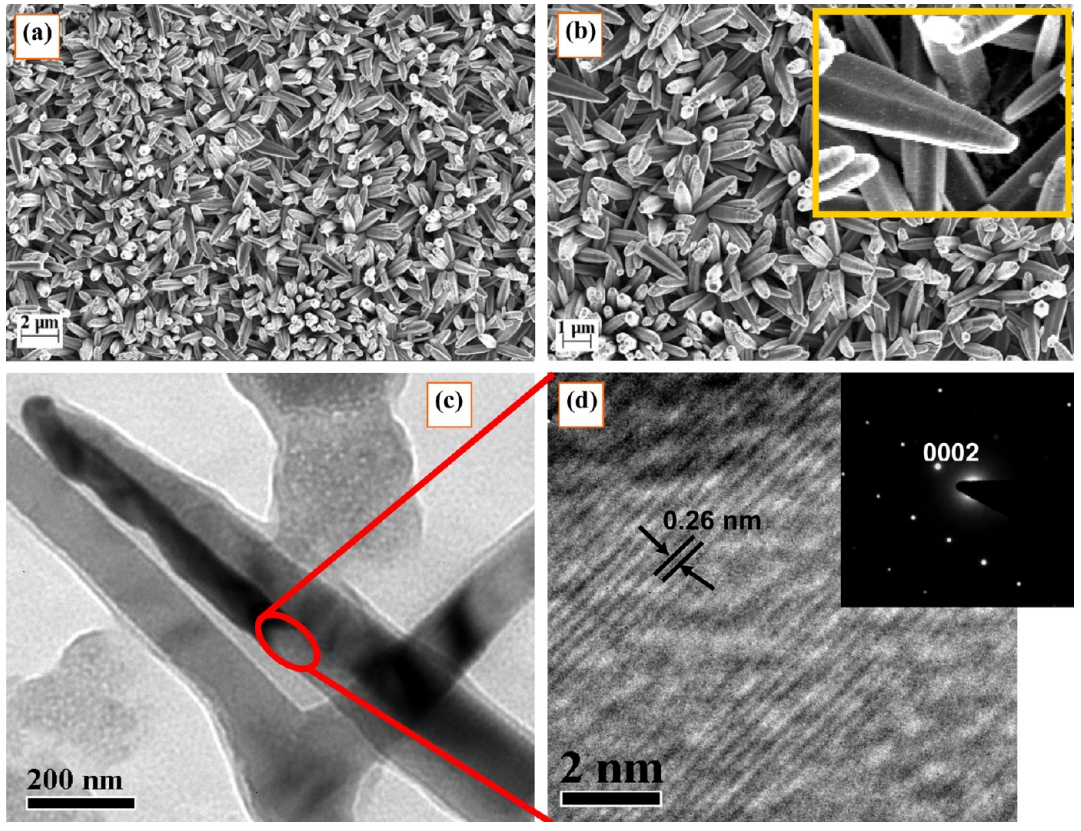

Figure 2. FESEM images of the grown ZnO nanostructures on copper substrate at (a) low- and (b) high-magnification. Inset shows magnified image of the micrograph. (c) TEM image of the grown ZnO nanorod; (d) the corresponding HRTEM image of the ZnO nanorod with SAED pattern in the inset.

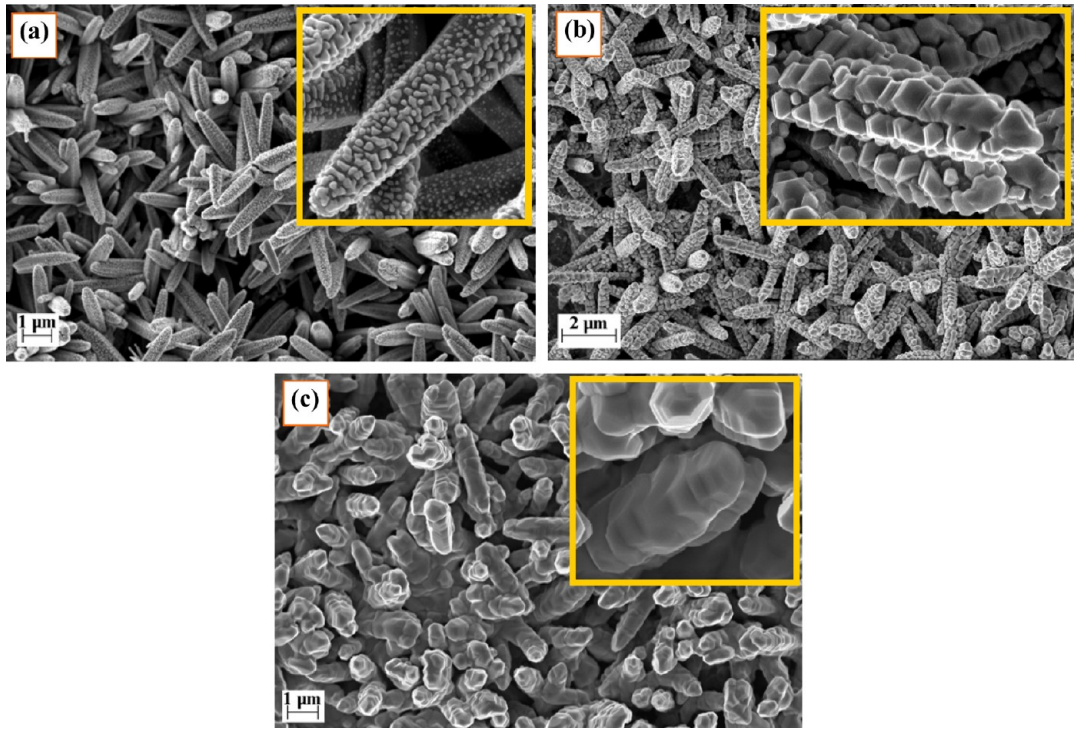

Figure 3. FESEM images of the grown CdS decorated ZnO nanorods on copper substrate, with deposition time of CdS of (a) 10, (b) 20, and (c) 30 min. Inset shows the magnified image of the micrograph.

crystallinity of the grown ZnO nanostructures. Figure 2c shows the TEM image of a nanorod with gradually decreasing tip diameter. Figure 2d reveals the HRTEM image of the portion encircled in Figure 2c, which demonstrates well-defined lattice

dx.doi.org/10.1021/am301721h | ACS Appl. Mater. Interfaces 2012, 4, 6085−6095

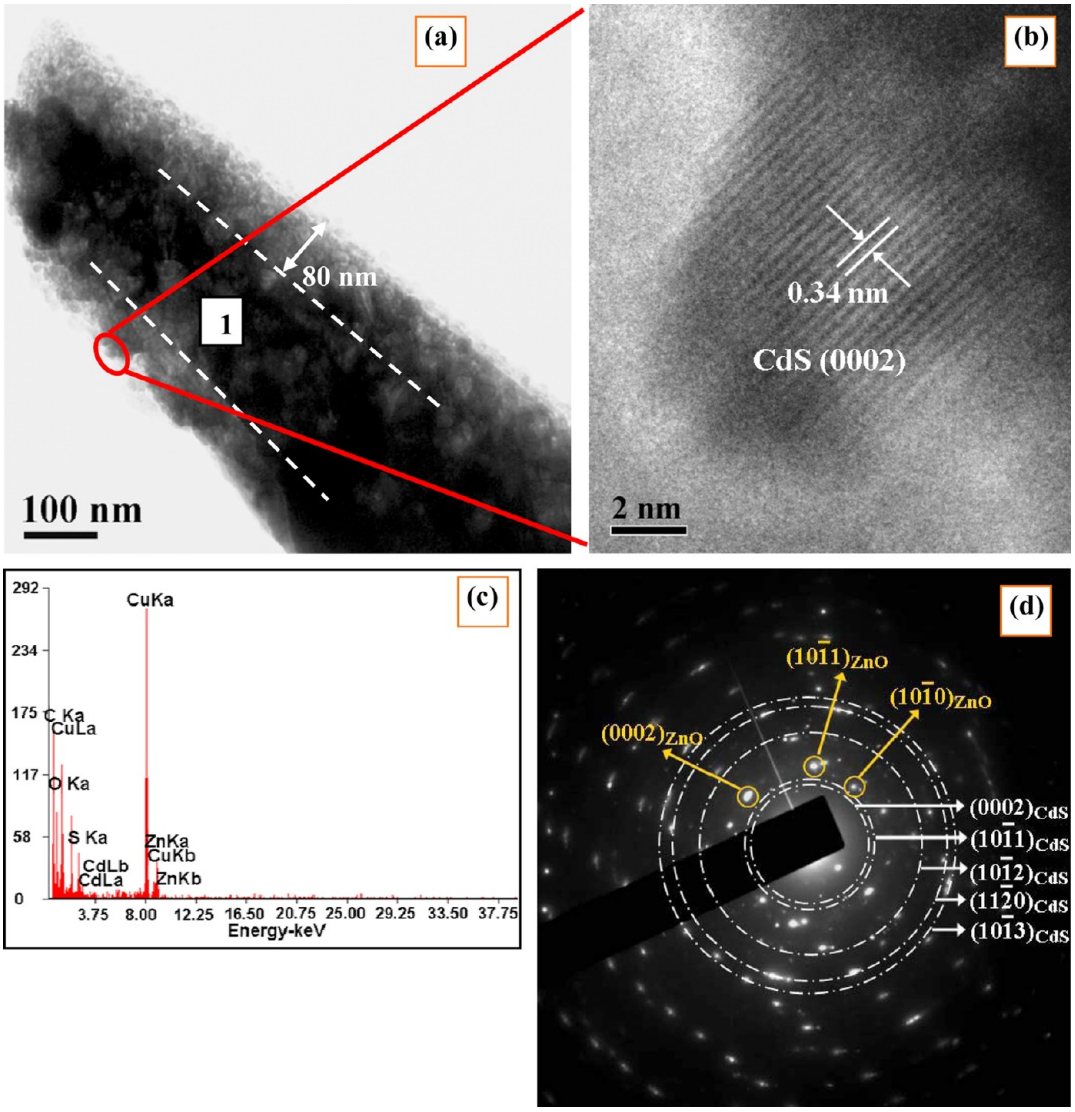

Figure 4. (a) TEM image of a fully CdS covered ZnO nanorod (CSZO-3 sample), (b) the corresponding HRTEM image of a CdS nanoparticle, (c) EDX (from region 1 shown in part a), and (d) corresponding SAED pattern of the nanorod. The dashed lines in a and d are intended to guide the eye.

fringes with the lattice spacing of 0.26 nm, in agreement with the spacing of the (0002) planes of the wurtzite ZnO.[40] It also indicates that the nanorods grow along the *c*-axis. The corresponding selected area electron diffraction (SAED) pattern, shown in the inset of Figure 2d, is also consistent with the HRTEM result.

Figure 3a–c shows the FESEM micrographs of CdS decorated ZnO nanorods on the copper substrate, grown at varying deposition time of CdS for 10, 20, and 30 min. The inset shows the magnified view of the micrographs. As revealed in Figure 3a, for the deposition time of 10 min, CdS nanoparticles are formed, which partially covers the surface of ZnO nanorods. When the deposition time is increased to 20 min, more CdS nanoparticles cover a larger surface area of the ZnO nanorods (Figure 3b). Figure 3c shows that the deposition time of 30 min produces much larger number of CdS nanoparticles, which merge to form a continuous layer to fully cover the surface of the ZnO nanorods. In the subsequent discussions, these CdS decorated ZnO nanorods, with deposition time of 10, 20, and 30 min, are referred to as sample CSZO-1, CSZO-2, and CSZO-3, respectively.

For a closer observation on the fully CdS covered ZnO nanorods, HRTEM was carried out on the CSZO-3 sample. Figure 4a shows the TEM image of a CdS decorated ZnO nanorod. As can be seen, a number of CdS nanoparticles, forming a continuous layer of ~80 nm thick, uniformly cover the surface of the ZnO nanorod. The HRTEM image in Figure 4b of a CdS nanoparticle (from the portion encircled in Figure 4a) reveals lattice fringes with a lattice spacing of 0.34 nm, which corresponds to the (0002) lattice planes of the wurtzite CdS.[41] Figure 4c presents the energy-dispersive X-ray spectroscopy (EDX) spectra of the CdS decorated ZnO nanorods (from region 1 of Figure 4a), which shows the presence of Zn, O, Cd, and S. The corresponding SAED pattern in Figure 4d displays a set of diffraction spots that originate from the single crystalline hexagonal ZnO core and several diffraction rings attributed to the polycrystalline hexagonal CdS shell. Thus, the TEM analysis reveals that polycrystalline hexagonal CdS uniformly covers the surface of the single crystalline ZnO nanorods for CSZO-3 sample.

Figure 5 shows the X-ray diffraction pattern of ZnO nanorods with and without CdS attachment. It is found that

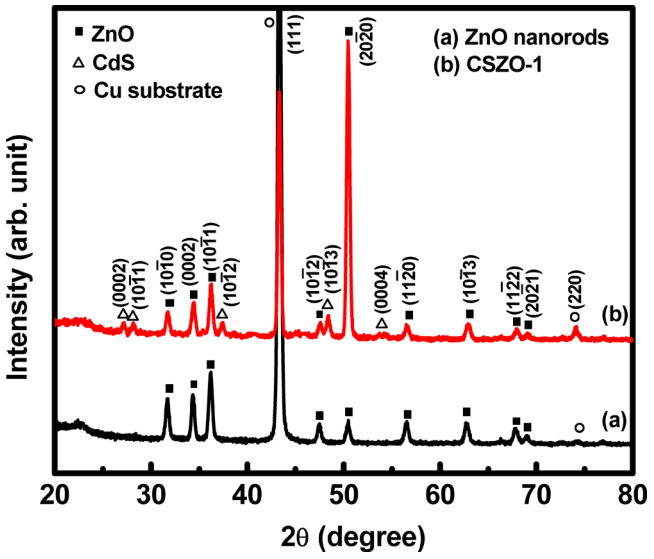

Figure 5. XRD pattern of the CdS modified and unmodified ZnO nanorods on copper substrate.

the CdS decorated ZnO nanorods consist of diffraction peaks corresponding to hexagonal CdS and wurtzite ZnO. The other peaks are attributed to the copper substrate. This result suggests that the deposited nanostructures are highly crystalline in nature.

The elemental bonding of the partially CdS covered ZnO nanorods was examined by XPS. The XPS spectrum of CSZO-1 sample with wide energy scan revealed the presence of elemental Zn, O, Cd, and S in the sample. The high-resolution XPS spectrum for each element is shown in Figure 6. The binding energy for Zn $2p_{3/2}$ electrons in Figure 6a, fitted by Gaussian curves, shows two peaks at 1021.3 eV and 1022.2 eV, which are associated with Zn^{2+} in ZnO wurtzite structure and zinc hydroxide species, respectively.[42−44] The O 1s electron binding energy peak, shown in Figure 6b, can be fitted well by three Gaussian components having centres at 530.1 eV, 531.3 eV, and 532.3 eV. The peak at 530.1 eV is assigned to the O 1s level in the ZnO structure, which is surrounded by the Zn atoms with their full complement of nearest-neighbor O^{2-} ions.[42,45] The peaks at 531.3 eV and 532.3 eV are related to the O 1s in the zinc hydroxide species[42,46] and adsorbed or chemisorbed oxygen species due to surface hydroxyl groups, respectively.[42,47,48] The spectrum of Cd 3d in Figure 6c shows two peaks at 405.4 and 412.1 eV, corresponding to the binding energy of Cd $3d_{5/2}$ and Cd $3d_{3/2}$ electrons, respectively in CdS.[49,50] Figure 6d shows the spectrum of S 2p electron peak at 162.4 eV, which corresponds to the binding energy of S 2p bonded in CdS.[50]

Both CdS-decorated and unmodified ZnO nanostructures were used for the fabrication of solar cell devices. To study the efficiency of electron-hole pair generation in ZnO:P3HT hybrid photovoltaic device, we used different organic solvents such as chlorobenzene, chloroform, and toluene. Figure 7a−c shows the ultraviolet−visible (UV−vis) absorption spectra of ZnO:P3HT hybrid blend in chlorobenzene, chloroform, and toluene solvents, respectively. It is found that the nature of the absorption spectra depends on the casting solvent and also on the variation in ZnO concentration in the blend. The figures reveal that the $\pi-\pi^*$ band of P3HT shows absorption only in the visible region (400−650 nm). There are three peaks located at 516, 555, and 604 nm, for all the films. The presence of three vibrational absorption peaks indicates that there is a strong interchain-interlayer interaction among the P3HT chains.[51] For the blend structure of ZnO:P3HT, the absorption is found in

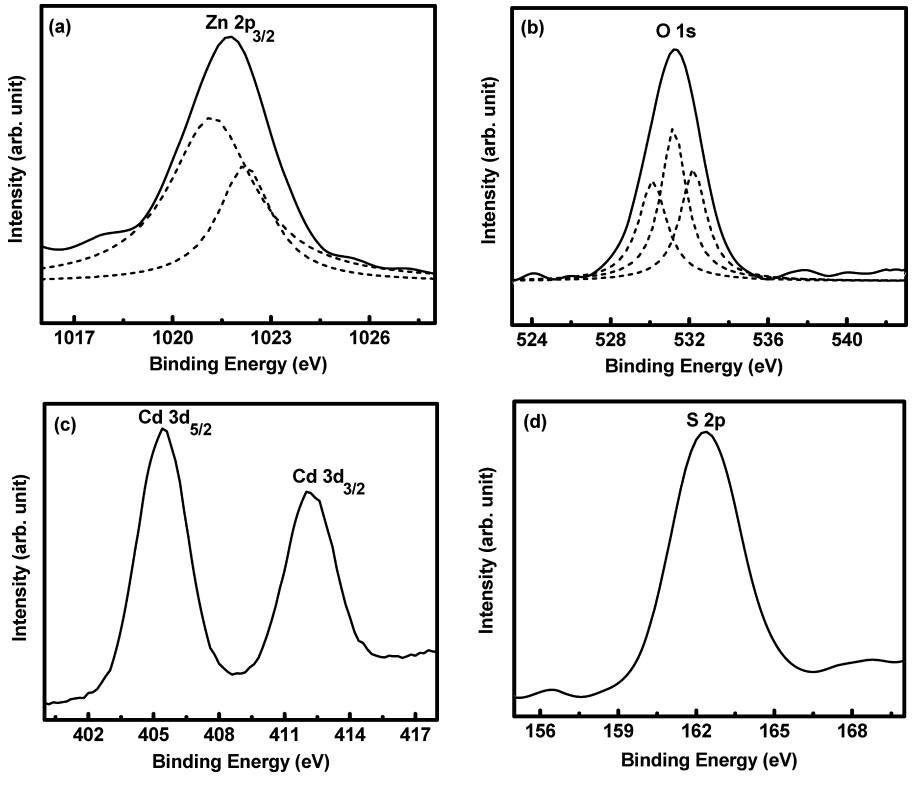

Figure 6. High-resolution XPS spectrum of (a) Zn, (b) O, (c) Cd, and (d) S, for partially CdS covered ZnO nanorods (CSZO-1 sample).

dx.doi.org/10.1021/am301721h | ACS Appl. Mater. Interfaces 2012, 4, 6085−6095

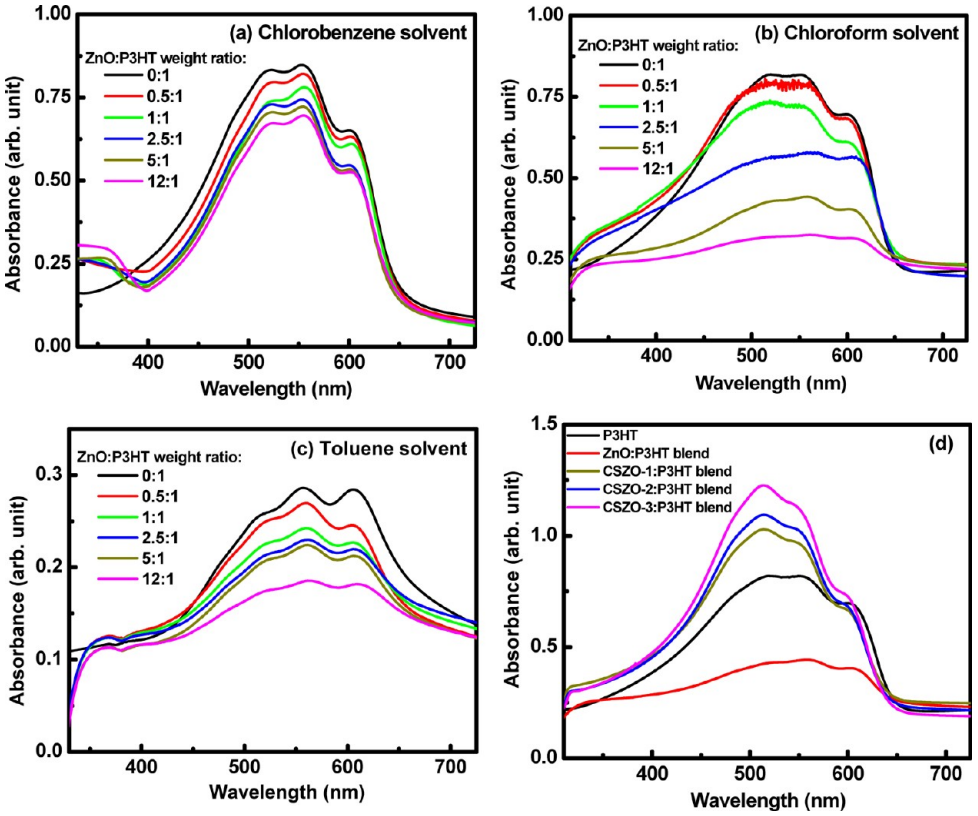

Figure 7. UV−vis absorption spectra of hybrid polymer ZnO:P3HT blend with different weight ratios, in solvents of (a) chlorobenzene, (b) chloroform, and (c) toluene. (d) UV−vis absorption spectra of P3HT, CdS modified ZnO:P3HT blend (of varying surface coverage of ZnO nanorods by CdS nanoparticles), and control ZnO:P3HT blend in chloroform solvent. The weight ratio of both ZnO:P3HT and CdS-modified ZnO:P3HT is 5:1.

the visible as well as in the ultraviolet region. This broadens the range of the absorption band. For the chlorobenzene-cast films, there is a drop in the absorption around 400 nm, which makes the peak in the ultraviolet and visible regions well distinguishable from each other. But for the chloroform-cast films, the P3HT appears to have a much broader peak, and the lowest absorbance is exhibited by toluene-cast films. With the increase in ZnO concentration in the ZnO:P3HT blend, the absorbance of P3HT gradually decreases and the rate of decrease is faster in chloroform-cast films than the others. However, three vibrational peaks of P3HT are still distinguishable for the blend films, which indicate a good polymer ordering in the blend films.[51] Figure 7d shows the UV−vis absorption spectra of CdS decorated ZnO nanorod:P3HT hybrid structure. For comparison, the spectra of P3HT and unmodified ZnO nanorods:P3HT of ZnO:P3HT weight ratio of 5:1 (similar to CdS modified one) in chloroform solvent are also presented. It reveals that the CdS modified ZnO device shows much higher absorption over the entire visible range than that of the unmodified ZnO one. It also shows a higher absorption in the range 300-580 nm as compared to P3HT. The absorption intensity is found to depend on the surface coverage of ZnO nanorods by CdS nanoparticles. With the increase in the surface coverage, the absorption intensity is also enhanced. The maximum absorption is observed when CdS fully covers the ZnO nanorods, i.e. for CSZO-3:P3HT sample. This enhanced absorption in the UV region is due to ZnO and that in the visible region is considered to be due to CdS nanostructures.

To study the effect of ZnO concentration and the solvent on the efficiency of charge generation and transfer, photoluminescence measurements were performed. Figure 8a−c shows the photoluminescence spectra of ZnO:P3HT blend in chlorobenzene, chloroform and toluene solvents, respectively. As seen in all cases, the photoluminescence intensity of P3HT is quenched by the addition of ZnO. This is due to the fast deactivation of the excited states by the electron-transfer reaction.[52] The quenching of emission owing to P3HT is enhanced with the increasing addition of ZnO. For ZnO:P3HT weight ratio of 0.5:1, 1:1, 2.5:1, 5:1, and 12:1, the photoluminescence intensity of P3HT is quenched by 55, 68, 75, 80, and 86%, respectively, for the chlorobenzene solvent. The corresponding values are found to be 57, 72, 76, 82, and 86% and 52, 63, 73, 79, and 85% for the chloroform and toluene solvents, respectively. This suggests that the ZnO nanorods behave as good electron acceptors when blended with P3HT. The residual PL is due to the excitons that are generated at a long distance from the ZnO:P3HT interface.[5] Thus increased quenching of the P3HT intensity with ZnO loading indicates the higher rate of dissociation of excitons. Also, as can be seen, at a particular ZnO concentration, the solvent plays an important role in the quenching mechanism. Highest PL quenching is observed for the chloroform-cast films, whereas the lowest one is observed for the toluene-cast films. High boiling point solvents like chlorobenzene (b.p. of 131°C) and toluene (b.p. of 110 °C) enhances the length of the conjugated chain making some of the photogenerated excitons unable to reach the neighboring ZnO molecules, as a result these excitons recombine radiatively, and give rise to the photoluminescence peak. But in lower boiling point solvent (chloroform), the donor and acceptor distributions are fast frozen and thus much

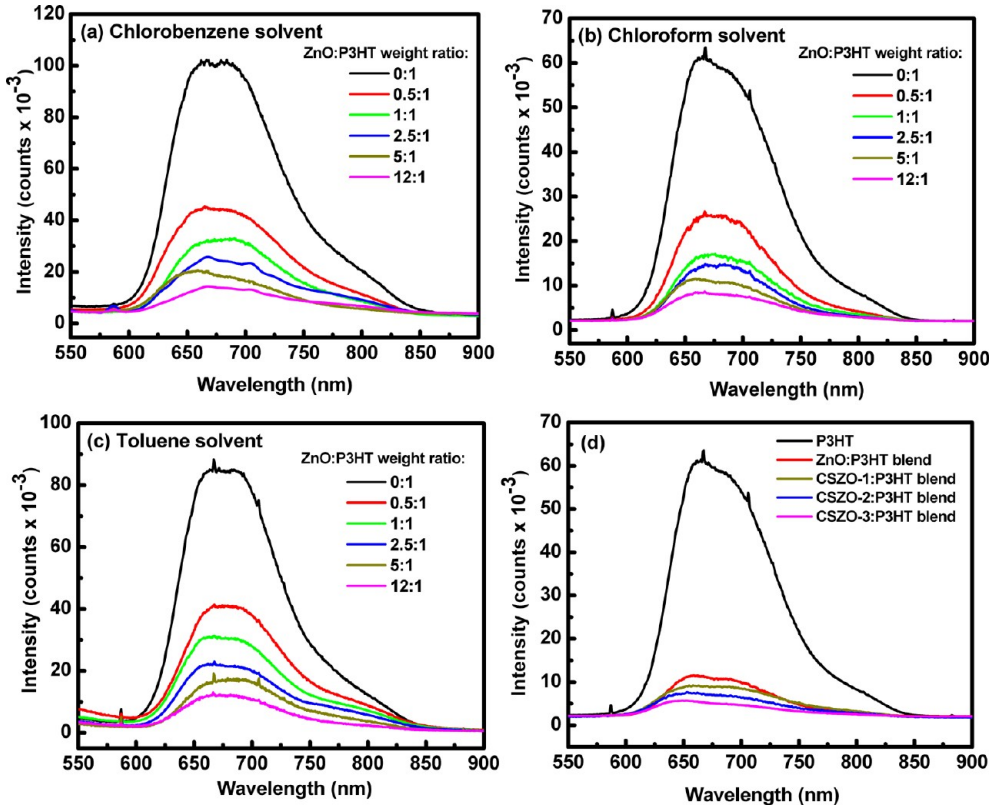

Figure 8. Photoluminescence spectra of hybrid polymer ZnO:P3HT blend with different weight ratios, in solvents of (a) chlorobenzene, (b) chloroform, and (c) toluene. (d) Photoluminescence spectra of P3HT, CdS-modified ZnO:P3HT blend (of varying surface coverage of ZnO nanorods by CdS nanoparticles), and control ZnO:P3HT blend in chloroform solvent. The weight ratio of both ZnO:P3HT and CdS-modified ZnO:P3HT is 5:1.

larger donor/acceptor interfaces are formed, leading to the dissociation of more photogenerated excitons. As a result, there is enhanced quenching in the photoluminescence intensity with the chloroform as the solvent.[52] Figure 8d compares the photoluminescence intensity of hybrid CdS decorated ZnO nanorods:P3HT along with that of P3HT and unmodified ZnO nanorods:P3HT blend in chloroform solvent. It is found that the quenching of the photoluminescence intensity of P3HT is enhanced by the addition of CdS on the surface of the ZnO nanorods. The quenching increases with the increase in surface coverage of ZnO nanorods by CdS nanoparticles. The photoluminescence intensity of P3HT is quenched by 85, 88, and 91% for the CSZO-1:P3HT, CSZO-2:P3HT, and CSZO-3:P3HT samples, respectively. Thus, the highest PL quenching is about 9% higher for the CdS decorated ZnO than that of the unmodified one.

The current density–voltage (J–V) characteristics of the ZnO:P3HT hybrid device using chlorobenzene, chloroform, and toluene solvents, measured under 100 mW/cm^2 AM 1.5 simulated solar irradiation condition are shown in Figure 9a–c, respectively. All the photovoltaic measurements have been carried out in air. The effect of ZnO concentration and casting solvent on the efficiency of the photovoltaic cells has been studied. As can be seen, for all the solvents, there is a gradual increase in short-circuit current density (J_{SC}) with the increase of ZnO concentration in the blend up to a ZnO:P3HT weight ratio of 5:1, but it decreases when the ratio is increased to 12:1. On the other hand, the open circuit voltage (V_{OC}) increases with the rise in ZnO concentration in the blend up to ZnO:P3HT weight ratio of 2.5:1, but gradually decreases thereafter. The fill factor (FF) and power conversion efficiency (PCE) follows the same trend as that of J_{SC}. The maximum PCE for each solvent is obtained when the ZnO:P3HT weight ratio is 5:1. The above results are summarized in Table 1. At a low ZnO concentration, the electron transport is relatively poor.[53] But with the increase of ZnO loading, an enhanced dissociation of photogenerated excitons takes place leading to larger number of electrons and holes. This generates more percolation pathways leading to the improved electron transport, and thus increased photocurrent. But the further increase of ZnO fraction in the blend film reduces the polymer content. Thus though the dissociation of more excitons occurs as revealed by the PL spectra (Figure 8a–c), the interpenetrating pathways for hole transport becomes poor.[54,55] As a result, the photocurrent decreases. Among the casting solvents, toluene shows the lowest PCE for each ZnO concentration, than that obtained using chlorobenzene and chloroform. The result can be well explained from the UV-visible and photoluminescence spectra. Toluene exhibited the lowest absorption among the solvents. Also, the quenching of photoluminescence intensity with the addition of ZnO is lower as compared to other solvents (chlorobenzene and chloroform), which indicates that lesser number of excitons are dissociated into electrons and holes. This may lower the efficiency of the toluene-cast films. Chloroform-cast films exhibit higher efficiency than the chlorobenzene-cast films. The efficiency has been found to be maximum for chloroform-cast film at ZnO:P3HT weight ratio of 5:1, and the corresponding values of photovoltaic parameters are: J_{sc} of 0.849 mA/cm^2, V_{oc} of 425 mV, FF of 32%, and PCE of 0.12%. Figure 9d shows the

dx.doi.org/10.1021/am301721h | ACS Appl. Mater. Interfaces 2012, 4, 6085–6095

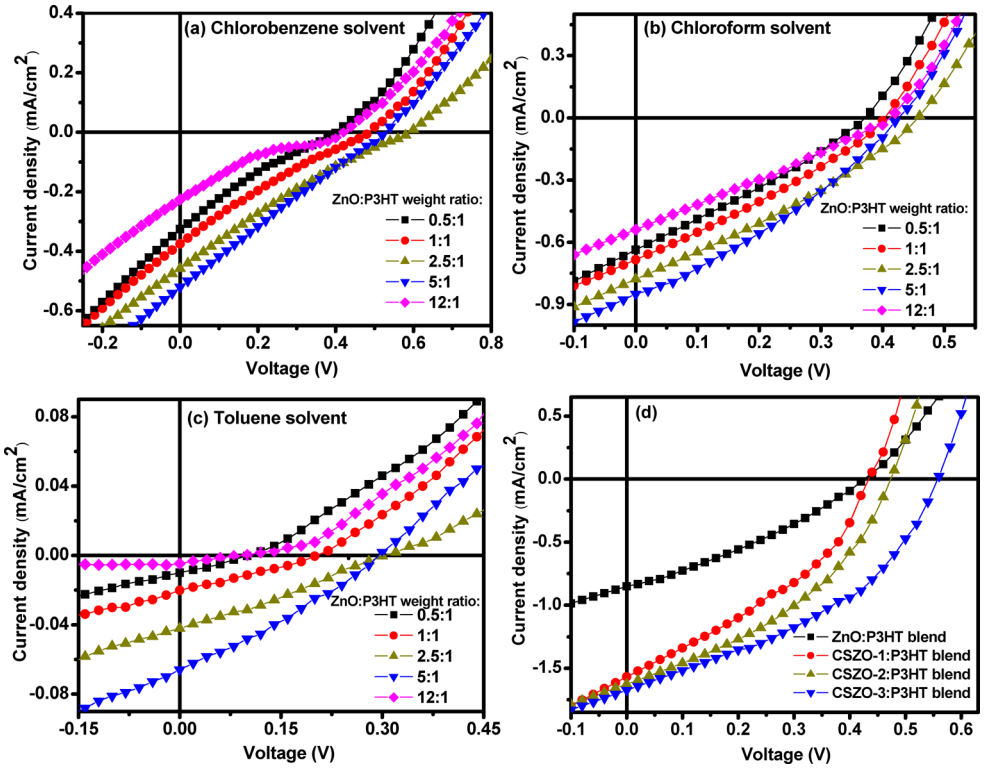

Figure 9. Current density–voltage characteristics of photovoltaic cells fabricated with hybrid polymer ZnO:P3HT blend with different weight ratios, in solvents of (a) chlorobenzene, (b) chloroform, and (c) toluene. (d) Current density–voltage characteristics of photovoltaic cells fabricated with CdS modified ZnO:P3HT blend (of varying surface coverage of ZnO nanorods by CdS nanoparticles) and control ZnO:P3HT blend in chloroform solvent. The weight ratio of both ZnO:P3HT and CdS modified ZnO:P3HT is 5:1.

Table 1. Photovoltaic Parameters Obtained for Solar Cells Fabricated with Hybrid Polymer ZnO:P3HT Blend with Different Weight Ratios and Using Different Casting Solvents

solvent	ZnO:P3HT weight ratio	short-circuit current density, J_{sc} (mA/cm^2)	open circuit voltage, V_{oc} (mV)	fill factor, FF (%)	efficiency, η (%)
chlorobenzene	0.5:1	0.325	402	20	0.03
	1:1	0.375	485	21	0.04
	2.5:1	0.458	590	21	0.06
	5:1	0.519	527	24	0.07
	12:1	0.226	417	17	0.02
chloroform	0.5:1	0.636	371	28	0.07
	1:1	0.684	403	29	0.08
	2.5:1	0.777	457	31	0.11
	5:1	0.849	425	32	0.12
	12:1	0.538	412	28	0.06
toluene	0.5:1	0.010	103	26	0.0003
	1:1	0.020	202	27	0.0011
	2.5:1	0.042	303	28	0.0036
	5:1	0.066	294	30	0.0058
	12:1	0.005	94	25	0.0001

current density–voltage (J–V) characteristics of the CdS decorated ZnO nanorods:P3HT hybrid device measured under the same condition. The characteristics for unmodified ZnO device of ZnO:P3HT weight ratio of 5:1 in chloroform solvent has also been plotted for comparison. The figure shows a clear increase in the J_{SC} and V_{OC} with the introduction of CdS nanoparticles on the surface of the ZnO nanorods. These parameters are again found to depend on the surface coverage of ZnO nanorods by CdS nanoparticles. With the increase in the surface coverage, J_{SC} increases by a small amount, but there is a noticeable increase in V_{OC}. The results obtained for CdS modified ZnO devices are summarized in Table 2. The photovoltaic parameters are found to be highest for CSZO-3:P3HT devices and the values are: J_{sc} of 1.674 mA/cm^2, V_{oc} of 557 mV, FF of 40%, and PCE of 0.38%. Thus, the maximum efficiency obtained for CdS decorated ZnO device is enhanced by more than 300% over the unmodified one.

The increase in V_{OC} and J_{SC} with the introduction of CdS nanoparticle can be well understood from the band diagram of Figure 10. For efficient transfer of electrons from donor to acceptor, the lowest unoccupied molecular orbital (LUMO) of donor have to be 0.3 to 0.5 eV higher than that of acceptor.[56] In ZnO:P3HT blend, this energy difference is 1.2 eV, which is much higher than that needed. The conduction band minimum

Table 2. Photovoltaic Parameters Obtained for Solar Cells Fabricated with Hybrid Polymer CdS-Decorated ZnO:P3HT Blend (of varying surface coverage of ZnO nanorods by CdS nanoparticles) with Weight Ratio of 5:1 and Using Chloroform As the Casting Solvent

device fabricated with blend	short-circuit current density, J_{sc} (mA/cm^2)	open circuit voltage, V_{oc} (mV)	fill factor, FF(%)	efficiency, η (%)
CSZO-1:P3HT	1.567	435	37	0.25
CSZO-2:P3HT	1.627	473	39	0.30
CSZO-3:P3HT	1.674	557	40	0.38

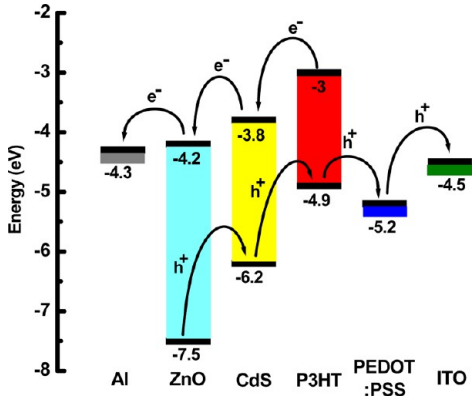

Figure 10. Schematic energy band diagram of the CdS-decorated ZnO:P3HT hybrid solar cell investigated in this study.

of CdS lies lower in energy than the LUMO of P3HT but higher than the conduction band of ZnO. So when CdS is introduced on the surface of ZnO nanorods, it creates a cascaded band structure, where electrons can easily transfer from P3HT to ZnO via CdS. Also, because of the valence band energy alignment of CdS relative to the highest occupied molecular orbital (HOMO) band of P3HT, CdS acts as a blocking layer by obstructing the transfer of holes from P3HT to ZnO, thus reducing the recombination and increasing the carrier lifetime. This efficient transfer of electrons together with reduced recombination increases the V_{OC} and J_{SC} in the CdS decorated ZnO devices. This process of electron transfer can be further improved by increasing the surface coverage of ZnO nanorods by CdS nanoparticles. When ZnO nanorods are only partially covered by CdS nanoparticles, in the uncovered portions, no cascaded band structure is formed, and the electron transfer occurs there in the same manner as in the unmodified devices. An increase in the number of nanoparticles results in an enhancement in the surface coverage of ZnO nanorods by CdS. When CdS fully covers the ZnO nanorods, the cascaded band structure is most efficiently formed. This increases the efficiency of electron transfer and the resultant V_{OC} and J_{SC}. All these factors result in enhancing the efficiency of CdS modified ZnO devices over the unmodified one. The above results appear to be corroborated by the photoluminescence spectra of Figure 8d, where it was found that the quenching of the photoluminescence intensity enhanced with the introduction of CdS on the ZnO nanorods. This implies that the electrons are more efficiently transferred in the CdS-modified ZnO devices, and the rate is enhanced with the increase in the surface coverage of ZnO nanorods by CdS nanoparticles.

The calculated external quantum efficiency (EQE) of ZnO:P3HT blend using chloroform as the casting solvent (as highest efficiency has been obtained using this solvent) is

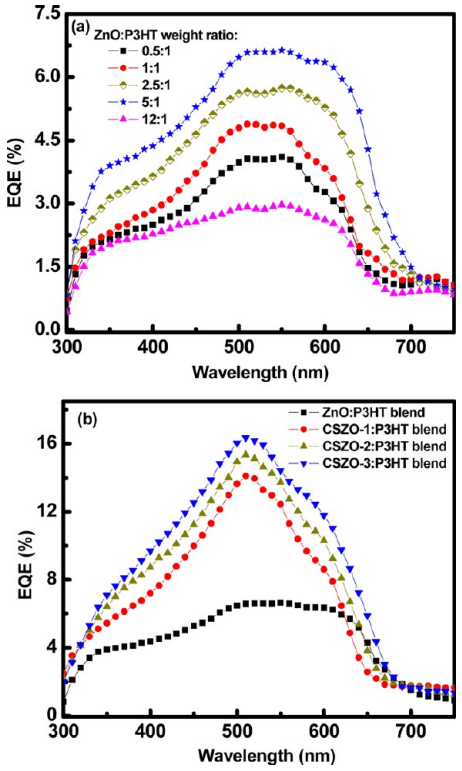

Figure 11. External quantum efficiency of the photovoltaic cells fabricated with hybrid polymer (a) ZnO:P3HT blend with different weight ratios, and (b) CdS-modified ZnO:P3HT blend (of varying surface coverage of ZnO nanorods by CdS nanoparticles) and control ZnO:P3HT blend. The weight ratio of both ZnO:P3HT and CdS modified ZnO:P3HT is 5:1. Chloroform has been used as the casting solvent in both a and b.

shown in Figure 11a. The EQE has been calculated using the relation

$$\mathrm{EQE}\ (\%) = \frac{100 \cdot 1240 \cdot J_{SC}}{\lambda P_0} \qquad (1)$$

where J_{SC} is the short-circuit current density (mA/cm^2), λ is the wavelength (nm) of incident radiation, and P_0 is the incident light intensity of the source (mW/cm^2). Each curve shows its respective highest EQE around 510 and 550 nm, with a shoulder peak around 600 nm. There is also a hump around 340 nm. This shows that the photocurrent action spectra closely follow the absorption spectra of the devices. With the increase of ZnO concentration (up to ZnO:P3HT weight ratio of 5:1), the EQE also increases. The highest EQE of ~7% is obtained for ZnO:P3HT weight ratio of 5:1 at around 510 and 550 nm. But for ZnO:P3HT weight ratio of 12:1, the EQE decreases to ~3%, which is least among all the films. Figure 11b shows the EQE of CdS decorated ZnO:P3HT device, along with that of unmodified one (of ZnO:P3HT weight ratio of 5:1). The CdS-modified ZnO device shows its highest peak at 510 nm, with shoulder peaks around 550 nm and 600 nm,

dx.doi.org/10.1021/am301721h | ACS Appl. Mater. Interfaces 2012, 4, 6085−6095

along with a hump around 340 nm. The EQE in the range 300−620 nm is much higher for the CdS-modified device than the unmodified one, and increases with the increase in the surface coverage of ZnO nanorods by CdS nanoparticles. The highest EQE value obtained at 510 nm is ∼16%, which is more than two times from that of the unmodified device.

CONCLUSIONS

We have fabricated hybrid photovoltaic devices based on active layers consisting of CdS modified and unmodified ZnO nanorods blended with P3HT. The optical and photovoltaic properties of these devices have been studied. It has been found that the CdS modified ZnO device shows a higher open circuit voltage, short-circuit current, and fill factor than that of unmodified one. This resulted in an increase in maximum efficiency by a factor of 3.0 for the CdS modified device. The experimental results show that with increase of ZnO concentration up to a certain amount in the blend, the efficiency of the cell increases. But the further increase of ZnO concentration decreases the polymer content in the film, so the pathway for hole transport becomes poor, which in turn decreases the efficiency of the cell. The casting solvent also plays an important role in governing the efficiency of the cell. In chloroform-cast films, more excitons dissociate into electrons and holes, which in turn increases the efficiency of the cells as compared to those of chlorobenzene and toluene-cast films. The absolute efficiency can be further increased with the introduction of a buffer layer at the interface of ZnO:P3HT blend and the top metal electrode, and if the photovoltaic devices are fabricated and measured under a controlled environment using a glove box.

AUTHOR INFORMATION

Corresponding Author

*E-mail: physkr@phy.iitkgp.ernet.in. Tel: +91-3222-283838. Fax: +91-3222-282700.

Notes

The authors declare no competing financial interest.

ACKNOWLEDGMENTS

This work was supported by DST SERI sponsored "NSH" project. The XPS facility of DST "FIST" project is also gratefully acknowledged.

REFERENCES

(1) Chan, M. Y.; Lai, S. L.; Fung, M. K.; Lee, C. S.; Lee, S. T. *Appl. Phys. Lett.* **2007**, *90*, 023504-1−023504-3.
(2) Chen, W. B.; Xiang, H. F.; Xu, Z. X.; Yan, B.-P.; Roy, V. A. L.; Che, C. M. *Appl. Phys. Lett.* **2007**, *91*, 191109-1−191109-3.
(3) Greenham, N. C.; Peng, X. G.; Alivisatos, A. P. *Phys. Rev. B* **1996**, *54*, 17628−17637.
(4) Ginger, D. S.; Greenham, N. C. *Phys. Rev. B* **1999**, *59*, 10622−10629.
(5) Beek, W. J. E.; Wienk, M. M.; Janssen, R. A. J. *Adv. Mater.* **2004**, *16*, 1009−1013.
(6) Beek, W. J. E.; Wienk, M. M.; Janssen, R. A. J. *Adv. Funct. Mater.* **2006**, *16*, 1112−1116.
(7) Coakley, K. M.; McGehee, M. D. *Appl. Phys. Lett.* **2003**, *83*, 3380−3382.
(8) Chang, C. H.; Huang, T. K.; Lin, Y. T.; Lin, Y. Y.; Chen, C. W.; Chu, T. H.; Su, W. F. *J. Mater. Chem.* **2008**, *18*, 2201−2207.
(9) Huynh, W. U.; Dittmer, J.; Alivisatos, A. P. *Science* **2002**, *295*, 2425−2427.
(10) Sun, B.; Snaith, H. J.; Dhoot, A. S.; Westenhoff, S.; Greenham, N. C. *J. Appl. Phys.* **2005**, *97*, 014914-1−014914-6.
(11) McDnoald, S. A.; Konstantatos, G.; Zhang, S.; Cyr, P. W.; Klem, E. J. D.; Levina, L.; Sargent, E. H. *Nat. Mater.* **2005**, *4*, 138−142.
(12) Liu, C.-Y.; Holman, Z. C.; Kortshagen, U. R. *Nano Lett.* **2009**, *9*, 449−452.
(13) Briseno, A. L.; Holcombe, T. W.; Boukai, A. I.; Garnett, E.C.; Shelton, S. W.; Fréchet, J. J. M.; Yang, P. *Nano Lett.* **2010**, *10*, 334−340.
(14) Bhat, S. V.; Govindaraj, A.; Rao, C. N. R. *Solar Energy Mater. Solar Cells* **2011**, *95*, 2318−2321.
(15) Zhang, Q.; Dandeneau, C. S.; Zhou, X.; Cao, G. *Adv. Mater.* **2009**, *21*, 4087−4108.
(16) Said, A. J.; Poize, G.; Martini, C.; Ferry, D.; Marine, W.; Giorgio, S.; Fages, F.; Hocq, J.; Bouclé, J.; Nelson, J.; Durrant, J. R.; Ackermann, J. *J. Phys. Chem. C* **2010**, *114*, 11273−11278.
(17) Erten-Ela, S.; Cogal, S.; Turkmen, G.; Icli, S. *Curr. Appl. Phys.* **2010**, *10*, 187−192.
(18) Lee, T.-H.; Sue, H.-J.; Cheng, X. *Nanotechnology* **2011**, *22*, 285401-1−6.
(19) Plass, R.; Pelet, S.; Krueger, J.; Gratzel, M.; Bach, U. *J. Phys. Chem. B* **2002**, *106*, 7578−7580.
(20) Kumar, A.; Jakhmola, A. *Langmuir* **2007**, *28*, 2915−2918.
(21) Diguna, L. J.; Shen, Q.; Kobayashi, J.; Toyoda, T. *Appl. Phys. Lett.* **2007**, *91*, 023116-1−023116-3.
(22) Leschkies, K. S.; Divakar, R.; Basu, J.; Enache-Pommer, E.; Boercker, J. E.; Carter, C. B.; Kortshagen, U. R.; Norris, D. J.; Aydil, E. S. *Nano Lett.* **2007**, *7*, 1793−1798.
(23) Peter, L.M.; Wijayantha, K.; Riley, D. J.; Waggett, J. P. *J. Phys. Chem. B* **2003**, *107*, 8378−8381.
(24) Zaban, A.; Micic, O. I.; Gregg, B. A.; Nozik, A. J. *Langmuir* **1998**, *14*, 3153−3156.
(25) Chang, C. H.; Lee, Y. L. *Appl. Phys. Lett.* **2007**, *91*, 053503-1−053503-3.
(26) Tachibana, Y.; Akiyama, H. Y.; Ohtsuka, Y.; Torimoto, T.; Kuwabata, S. *Chem. Lett.* **2007**, *36*, 88−89.
(27) Nozik, A. J. *Physica E* **2002**, *14*, 115−120.
(28) Zhai, T. Y.; Fang, X. S.; Bando, Y.; Dierre, B.; Liu, B. D.; Zeng, H. B.; Xu, X. J.; Huang, Y.; Yuan, X. L.; Sekiguchi, T.; Golberg, D. *Adv. Funct. Mater.* **2009**, *19*, 2423−2430.
(29) Zhang, M.; Zhai, T. Y.; Wang, X.; Liao, Q.; Ma, Y.; Yao, J. N. *J. Solid State Chem.* **2009**, *182*, 3188−3194.
(30) Mondal, S. P.; Ray, S. K. *Proc. Natl. Acad. Sci. India, A* **2012**, *82*, 21−29.
(31) Mondal, S. P.; Ray, S. K. *Appl. Phys. Lett.* **2009**, *94*, 223119-1−223119-3.
(32) Fang, F.; Zhao, D. X.; Li, B. H.; Zhang, Z. Z.; Zhang, J. Y.; Shen, D. Z. *Appl. Phys. Lett.* **2008**, *93*, 233115-1−233115-3.
(33) Wang, X.; Liu, G.; Lu, G. Q.; Cheng, H.-M. *Int. J. Hydrogen Energy* **2010**, *35*, 8199−8205.
(34) Spoerke, E. D.; Lloyd, M. T.; McCready, E. M.; Olson, D. C.; Lee, Y.-J.; Hsu, J. W. P. *Appl. Phys. Lett.* **2009**, *95*, 213506-1−213506-3.
(35) Luan, C.; Vaneski, A.; Susha, A. S.; Xu, X.; Wang, H.-E.; Chen, X.; Xu, J.; Zhang, W.; Lee, C.-S.; Rogach, A. L.; Zapien, J. A. *Nanoscale Res. Lett.* **2011**, *6*, 340-1−8.
(36) Tak, Y.; Hong, S. J.; Lee, J. S.; Yong, K. *J. Mater. Chem.* **2009**, *19*, 5945−5951.
(37) Guerguerian, G.; Elhordoy, F.; Pereyra1, C. J.; Marotti, R. E.; Martín, F.; Leinen, D.; Ramos-Barrado, J. R.; Dalchiele, E. A. *Nanotechnology* **2011**, *22*, 505401-1−9.
(38) Sun, B.; Hao, Y.; Guo, F.; Cao, Y.; Zhang, Y.; Li, Y.; Xu, D. *J. Phys. Chem. C* **2012**, *116*, 1395−1400.
(39) Rakshit, T.; Mandal, S.; Mishra, P.; Dhar, A.; Manna, I.; Ray, S. K. *J. Nanosci. Nanotechno.* **2012**, *12*, 308−315.
(40) Li, C.; Lei, W.; Zhang, X.; Wang, J. X.; Sun, X. W.; Tan, S. T. *J. Vac. Sci. Technol. B* **2007**, *25*, 590−593.
(41) Seol, M.; Kim, H.; Tak, Y.; Yong, K. *Chem. Commun.* **2010**, *46*, 5521−5523.

(42) Sepulveda-Guzman, S.; Reeja-Jayan, B.; de la Rosa, E.; Torres-Castro, A.; Gonzalez-Gonzalez, V.; Jose-Yacamane, M. *Mater. Chem. Phys.* **2009**, *115*, 172−178.
(43) De la Rosa, E.; Sepúlveda-Guzman, S.; Reeja-Jayan, B.; Torres, A.; Salas, P.; Elizondo, N.; Jose Yacaman, M. *J. Phys. Chem. C* **2007**, *111*, 8489−8495.
(44) Dake, L. S.; Baer, D. R.; Zachara, J. M. *Surf. Interface Anal.* **1989**, *14*, 71−75.
(45) Ramgir, N. S.; Mulla, I. S.; Pillai, V. K. *J. Phys. Chem. B* **2006**, *110*, 3995−4001.
(46) Wagner, C. D.; Passoja, D. E.; Hillery, H. F.; Kinisky, T. G.; Six, H. A.; Jansen, W. T.; Taylor, J.A. *J. Vac. Sci. Technol.* **1982**, *21*, 933−944.
(47) Ramgir, N. S.; Late, D. J.; Bhise, A. B.; More, M. A.; Mulla, I. S.; Joag, D. S.; Vijayamohanan, K. *J. Phys. Chem. B* **2006**, *110*, 18236−18242.
(48) Li, Z.; Xiong, Y.; Xie, Y. *Inorg. Chem.* **2003**, *42*, 8105−8109.
(49) Stoev, M.; Katerski, A. *J. Mater. Chem.* **1996**, *6*, 377−380.
(50) Wang, W.; Liu, Z.; Zheng, C.; Xu, C; Liu, Y.; Wang, G. *Mater. Lett.* **2003**, *57*, 2755−2760.
(51) Li, G.; Shrotriya, V.; Huang, J.; Yao, Y.; Moriarty, T.; Emery, K.; Yang, Y. *Nat. Mater.* **2005**, *4*, 864−868.
(52) Yu, H. *Synth. Met.* **2010**, *160*, 2505−2509.
(53) Beek, W. J. E.; Wienk, M. M.; Kemerink, M.; Yang, X.; Janssen, R. A. J. *J. Phys. Chem. B* **2005**, *109*, 9505−9516.
(54) Freitas, J. N. de; Grova, I. R.; Akcelrud, L. C.; Arici, E.; Sariciftci, N. S.; Nogueira, A.F. *J. Mater. Chem.* **2010**, *20*, 4845−4853.
(55) Lee, H.; Kim, S.; Chung, W.-S.; Kim, K.; Kim, D. *Sol. Energy Mater. Sol. Cells* **2011**, *95*, 446−452.
(56) Sandberg, H. G. O.; Frey, G. L.; Shkunov, M. N.; Sirringhaus, H.; Friend, R. H.; Nielsen, M. M.; Kumpf, C. *Langmuir* **2002**, *18*, 10176−10182.